Supplementary Information of "Proton Surface Exchange Kinetics of Perovskite Triple Conducting Thin Films for Protonic Ceramic Electrolysis Cells: $BaPr_{0.9}Y_{0.1}O_{3-\delta}$ (BPY) *vs.* $Ba_{1-x}Co_{0.4}Fe_{0.4}Zr_{0.1}Y_{0.1}O_{3-\delta}$ (BCFZY)"

Jongmin Lee[1,2], Haley B. Buckner[1,2] and Nicola H. Perry[1,2,*]

[1]Department of Materials Science & Engineering, University of Illinois Urbana-Champaign, 1304 W. Green St., Urbana, IL 61801, United States of America

[2]Materials Research Laboratory, University of Illinois Urbana-Champaign, 104 S. Goodwin Ave., Urbana, IL 61801, United States of America

*Corresponding Author E-mail: nhperry@illinois.edu
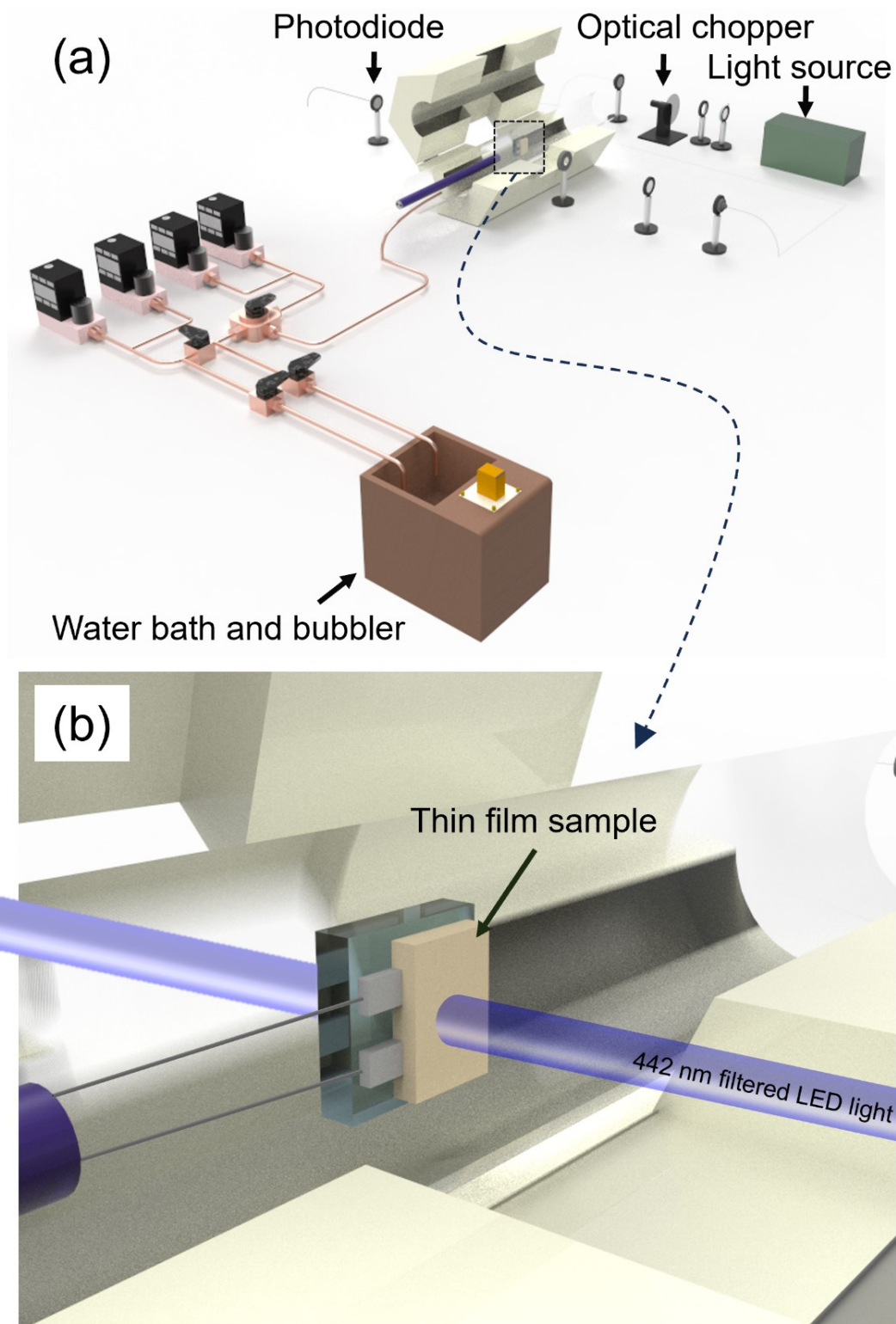
Supplementary Figure S1 (a) Schematic of OTR and ECR setup for steam relaxation measurements. (b) Well-defined thin film structure and buried Pt current collector inside quartz tube in the optical furnace.
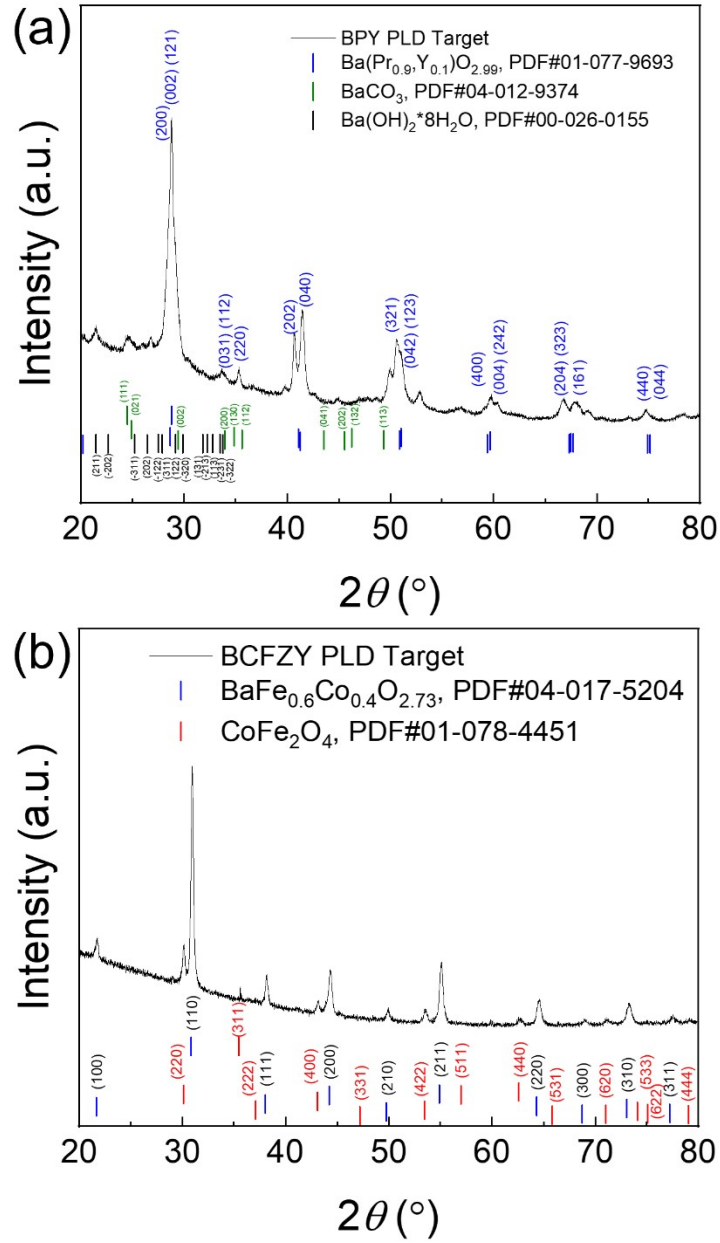
Supplementary Figure S2 X-ray patterns of BPY (a) and BCFZY (b) PLD ceramic targets. Vertical bar positions are marked with the PDF references.
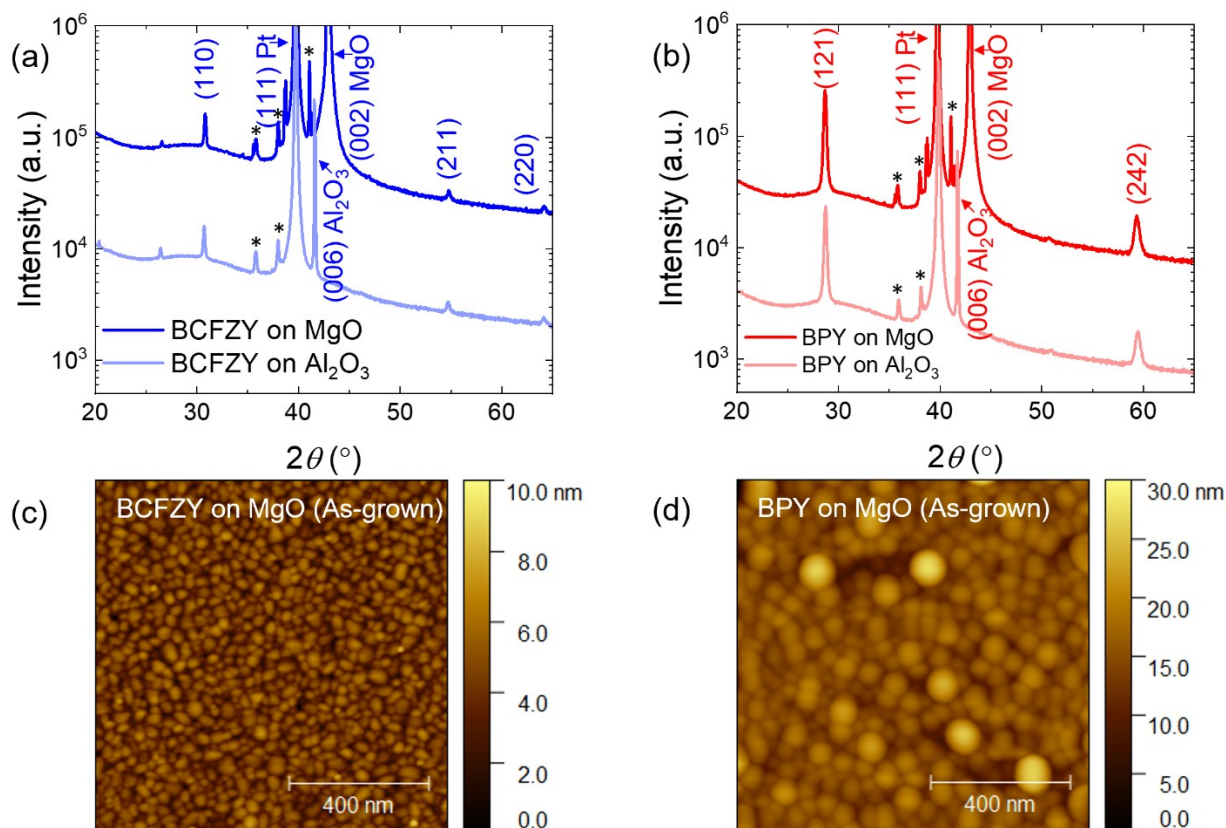
Supplementary Figure S3 XRD patterns (a),(b) and topographic AFM surface images (c),(d) of BCFZY and BPY thin films, respectively, grown on MgO and Al_2O_3 (001) substrates (as-deposited). The thicknesses of BCFZY and BPY are ~ 150 and 200 nm, respectively. Note that asterisks are from the diffraction peaks of $(111)_{Pt}$ and $(002)_{MgO}$ reflected by residual Cu_kβ (λ = 1.392 Å) and W_Lα (λ = 1.4767 Å) radiation. The rms roughnesses of BCFZY and BPY thin films are 0.593 and 1.512 nm, respectively, and estimated mean grain sizes of BCFZY and BPY thin films are 29.37 and 42.89 nm, respectively.

Discussion of Optical Changes Upon H Incorporation

We have run *ex-situ* UV-vis spectroscopy on a nominally dry then H-incorporated BPY film (annealed in steam at 0.21 atm at intermediate temperature then quenched) and found a broad decrease in optical absorption over a wide energy range (at least between 2 and 3 eV) for the H-incorporated sample. These broad decreases in absorption over wide energy ranges have been observed in our prior work on mixed conductors when hole concentration decreases. [1] Generally, optical transmitted intensity changes at elevated temperatures are related to redox processes in mixed ionic electronic conductors. [2] In the present work, the optical transmitted intensity increase, just like the electrical resistance increase, is thought to be related to the decrease in hole concentration as pH$_2$O is increased, with equal optical and electrical time constants (within fitting error). During hydrogenation holes in the p-type material are consumed [H_2O $(g) + 2O_O^{\times} + 2h^{\bullet} \rightarrow 2(OH)_O^{\bullet} + 1/2O_2 (g)$], likely leading to a rise in the Fermi level.

At a simplified level, optical absorption changes may be attributable to these shifts in the Fermi level with redox. Charge-transfer transitions into empty states at the top of the valence band in p-type systems or into empty states within impurity bands can be quenched as the material reduces and the Fermi level rises, filling the empty states. The optical absorption spectrum of nominally undoped BaPrO$_3$ is reportedly complex, giving rise to uncertainty in the optical band gap and the origins of intermediate energy absorption [3]. The valence band of the acceptor-doped counterpart in this work, BPY, is thought to have significant O 2p character according to our prior studies, with probable partial Pr 4f hybridization [4,5]. The top of the valence band might contain unoccupied states, which would enable optical absorption from charge transfer transitions when the Fermi level is positioned within the valence band. On the other hand, this particular sub-gap optical transition would disappear if the valence band states are full, when Fermi level is moved upwards. While we suggest significant O 2p character of the holes (O$^{2-/1-}$), it is possible that Pr 4f holes may contribute to some extent (Pr$^{3+/4+}$ redox). (A similar process could in principle take place if an intermediate band is formed by Pr states, although our prior work does not point to this electronic structure.) However, this explanation is a very simplified, hypothetical picture assuming rigid band Fermi level shifts, which probably does not reflect the full situation: the electronic structure likely changes as protons are incorporated. The origin of optical absorption in the BPY thin film regarding the hydrogenation/dehydrogenation process needs to be further studied, building on our prior electronic structure calculations in the non-protonated (dry) state.
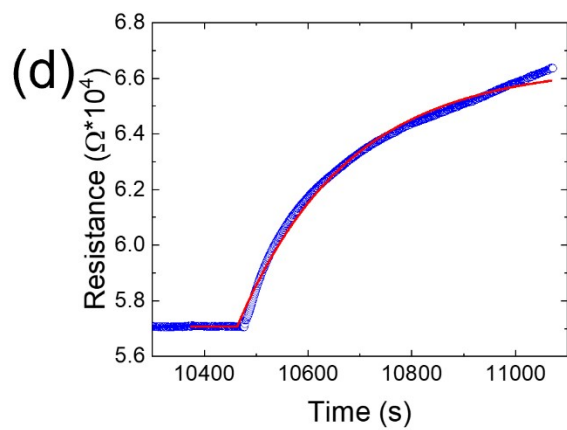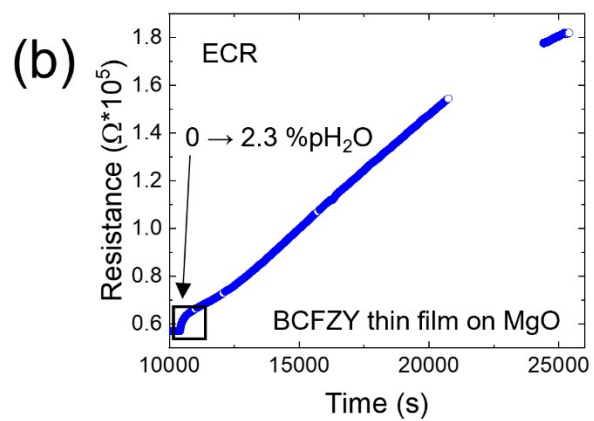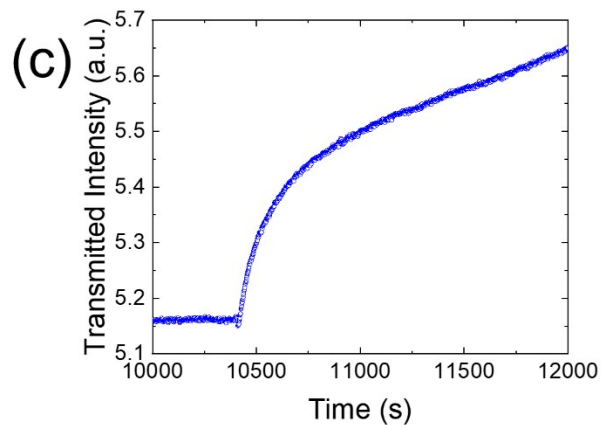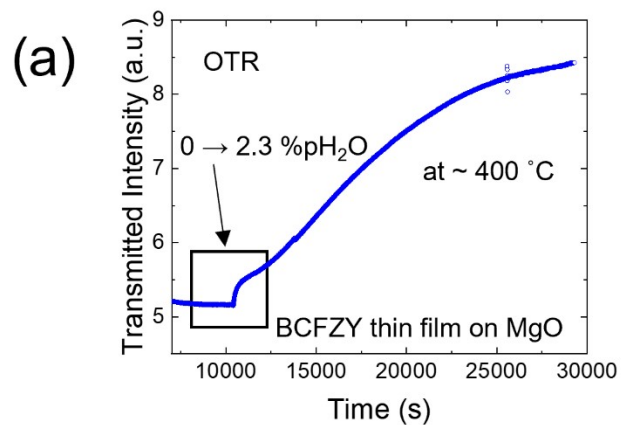
Discussion of Thickness Dependence

We compared the k values of the BPY thin films with different thicknesses of ~ 75 and ~ 320 nm grown on MgO substrates. From fits of the OTR curves shown in Supplementary Figure S4, the $(1/\tau)$ values are 0.02619 and 0.09327 s^{-1}, respectively. Since k values are calculated from fit curves by an equation of $k = L/\tau$, where L is the thickness, and τ is the time constant, the calculated k values of BPY thin films show $7.0*10^{-7}$ and $8.38*10^{-7}$ cm/s for the thicknesses of 75 and 320 nm, respectively. They show 8.3% difference between them. Considering the $\pm 20\%$ error in the k values, the sample thickness does not influence the proton surface exchange coefficients in the BPY thin films. Furthermore, the critical thickness (L_c) of proton surface exchange reaction is theoretically calculated by $L_c = D/k$, where D is diffusion coefficient [cm^2/s], k is surface exchange coefficient [cm/s]. Based on those values (D: $10^{-5} \sim 10^{-4}$ cm^2/s, k: $10^{-4} \sim 10^{-3}$ cm/s) from the literature [6] for $BaZr_{0.2}Ce_{0.65}Y_{0.15}O_{3-d}$ (BZCY) perovskite structure instead of BPY, the critical thickness is estimated to be 1000 μm, which is many orders of magnitude larger than the film thickness. Hence, the proton incorporation kinetics are limited by surface exchange in our work.
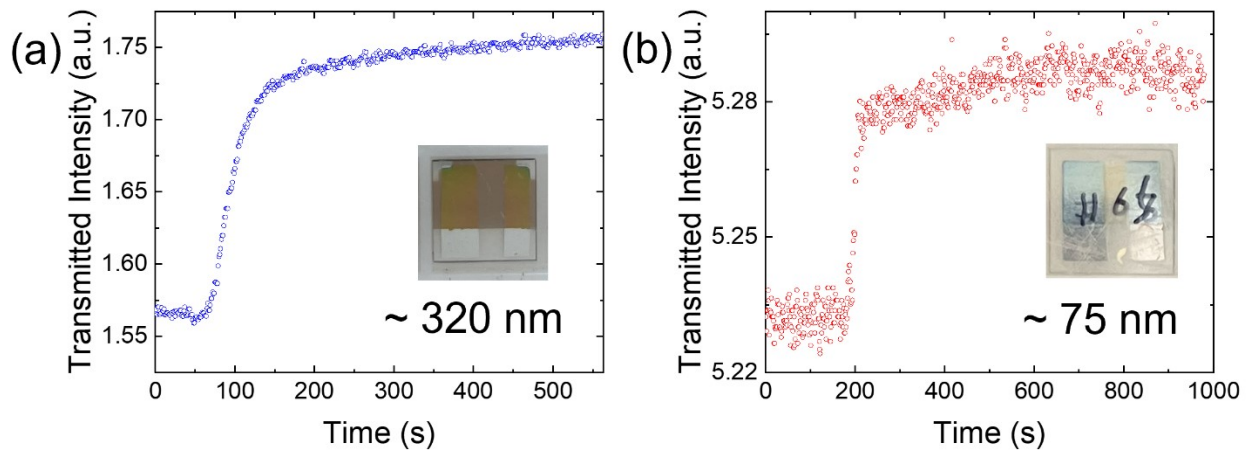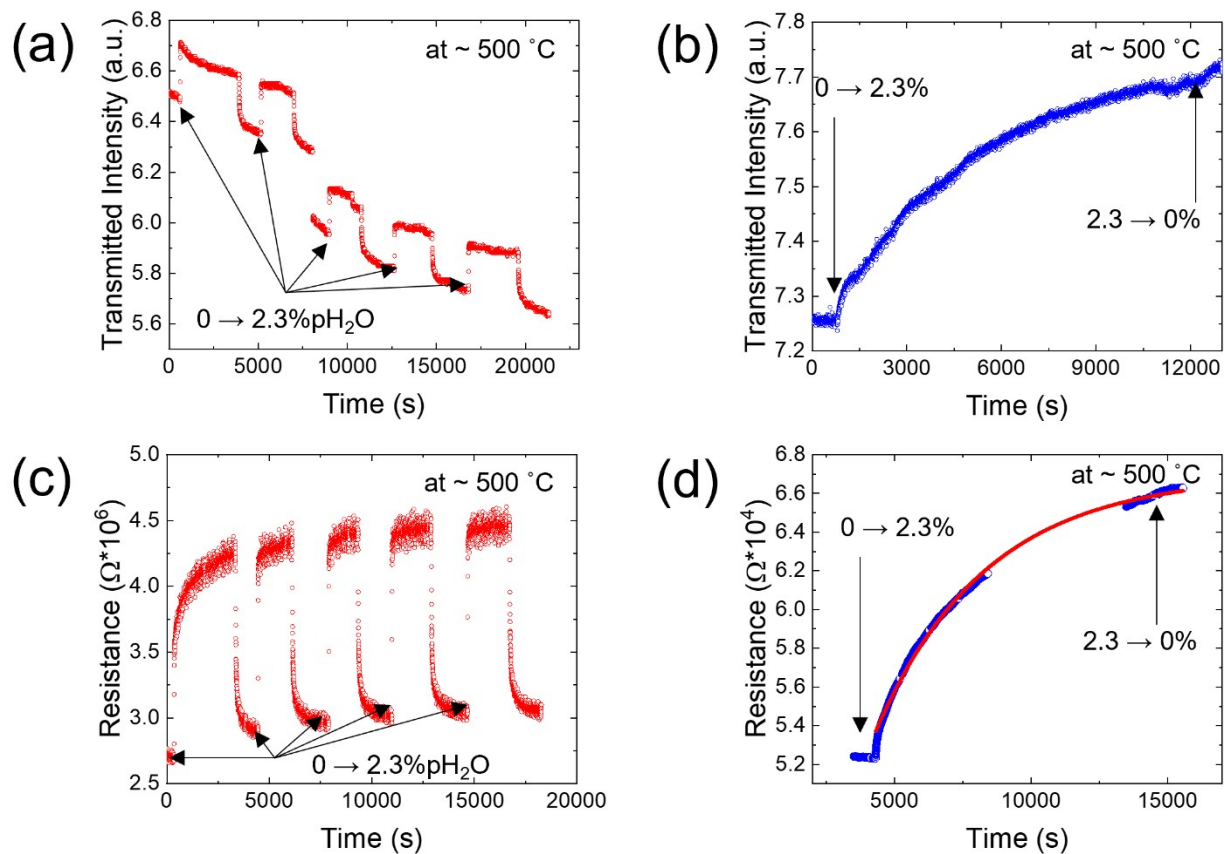

Supplementary Figure S4 OTR and fit curves at 400 ˚C as a function of time for the BPY thin films with thicknesses of 320 (a),(c) and 75 (b),(d) nm grown on MgO substrate.
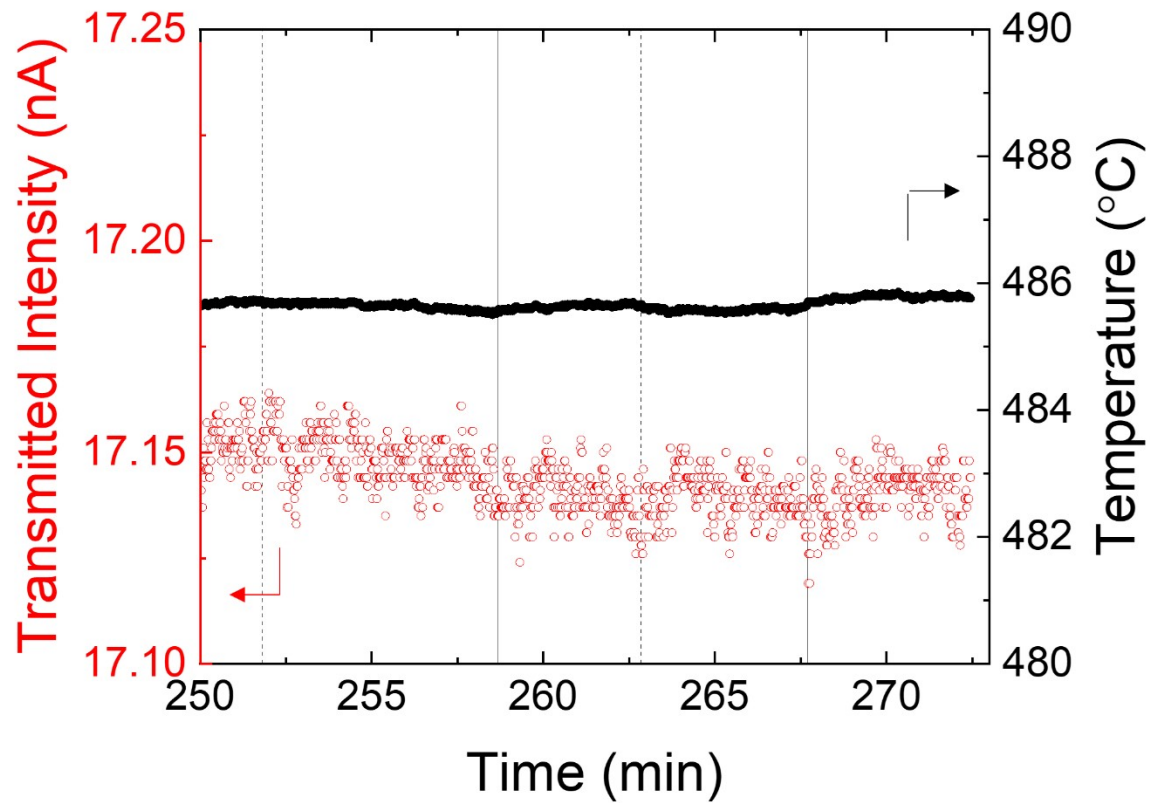
Supplementary Figure S5 Optical transmitted light intensity of double-side polished *c*-cut sapphire substrate at a temperature of ~ 486 ˚C. Dashed and solid lines represent steam switching from 0 to 2.3 %pH$_2$O and 2.3 to 0 %pH$_2$O, respectively.

Supplementary Figure S6 Repeatable OTR curves at 400 °C as a function of time (a), separated OTR curves (b)-(g), and corresponding fits (h)-(m) for the BPY thin film grown on MgO substrate.
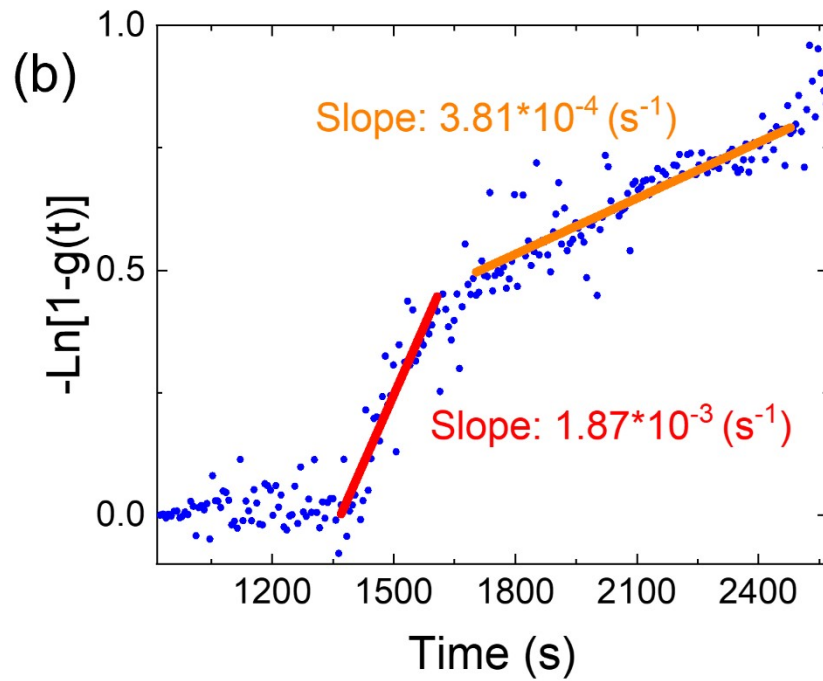
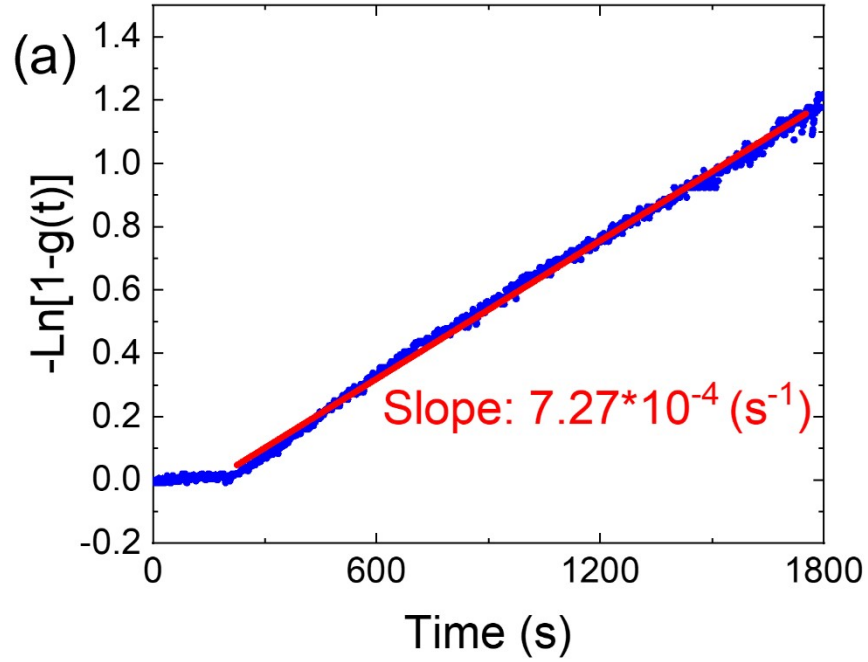**Supplementary Figure S7** OTR (a) and ECR (b) curves of BCFZY thin film grown on MgO substrate. Figure S7 (c) and (d) show enlarged square when steam switching in Figure S7 (a) and (b), respectively.

**Supplementary Figure S8** OTR and ECR curves of replicates BPY (a),(c) and BCFZY (b),(d) thin films during steam switching as a function of time at a constant temperature of approximately 500 ˚C.
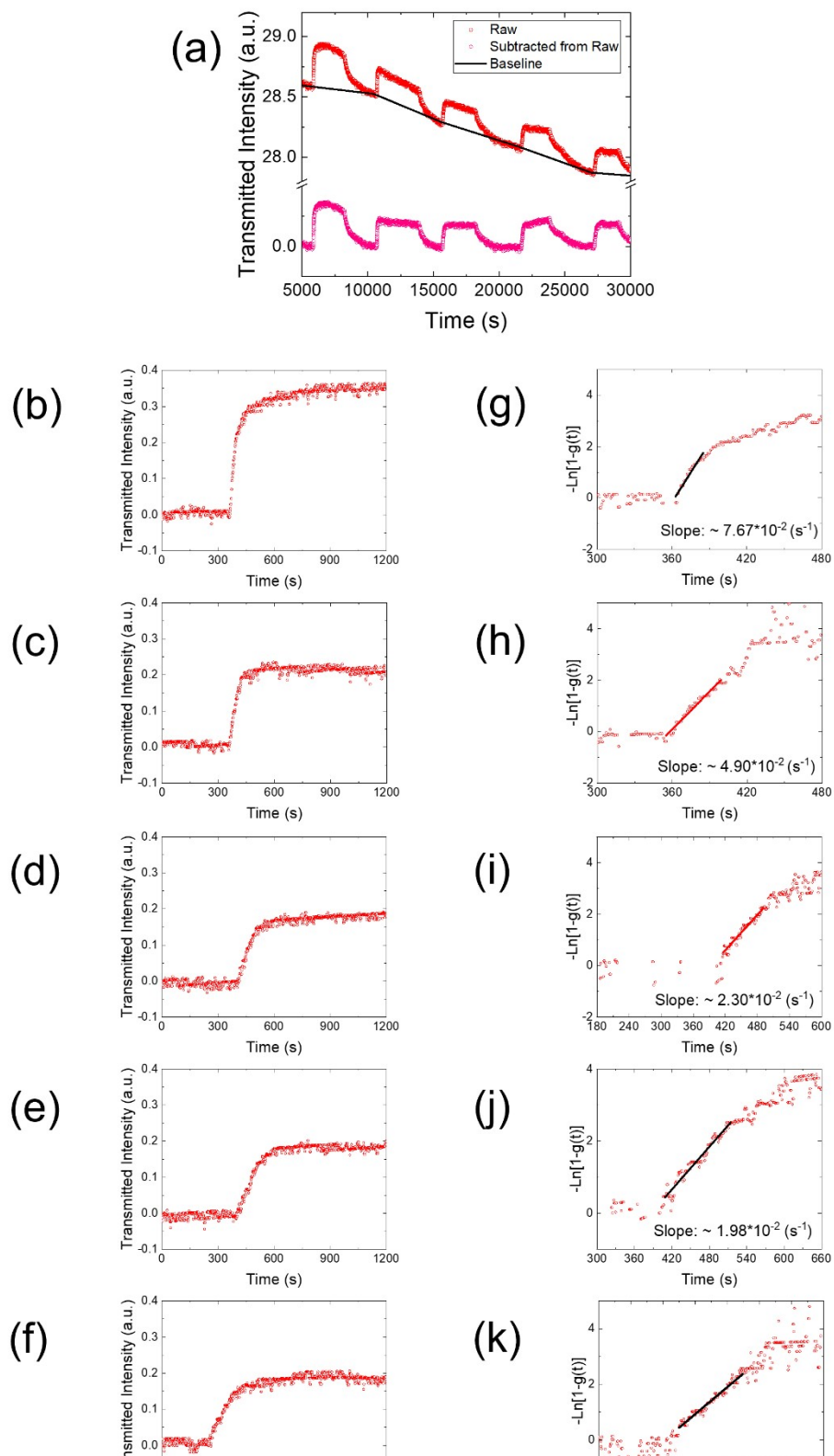
Supplementary Figure S9 (a) OTR curves upon pH$_2$O switching as a function of time and baseline subtracted OTR curves (b)-(f) and corresponding fits (g)-(k) for the BPY thin film grown on sapphire at a constant temperature of ~ 400 ˚C.

Supplementary Figure S10 Fits of OTR and ECR curves for the BCFZY thin film grown on sapphire at a constant temperature of ~ 400 ˚C.
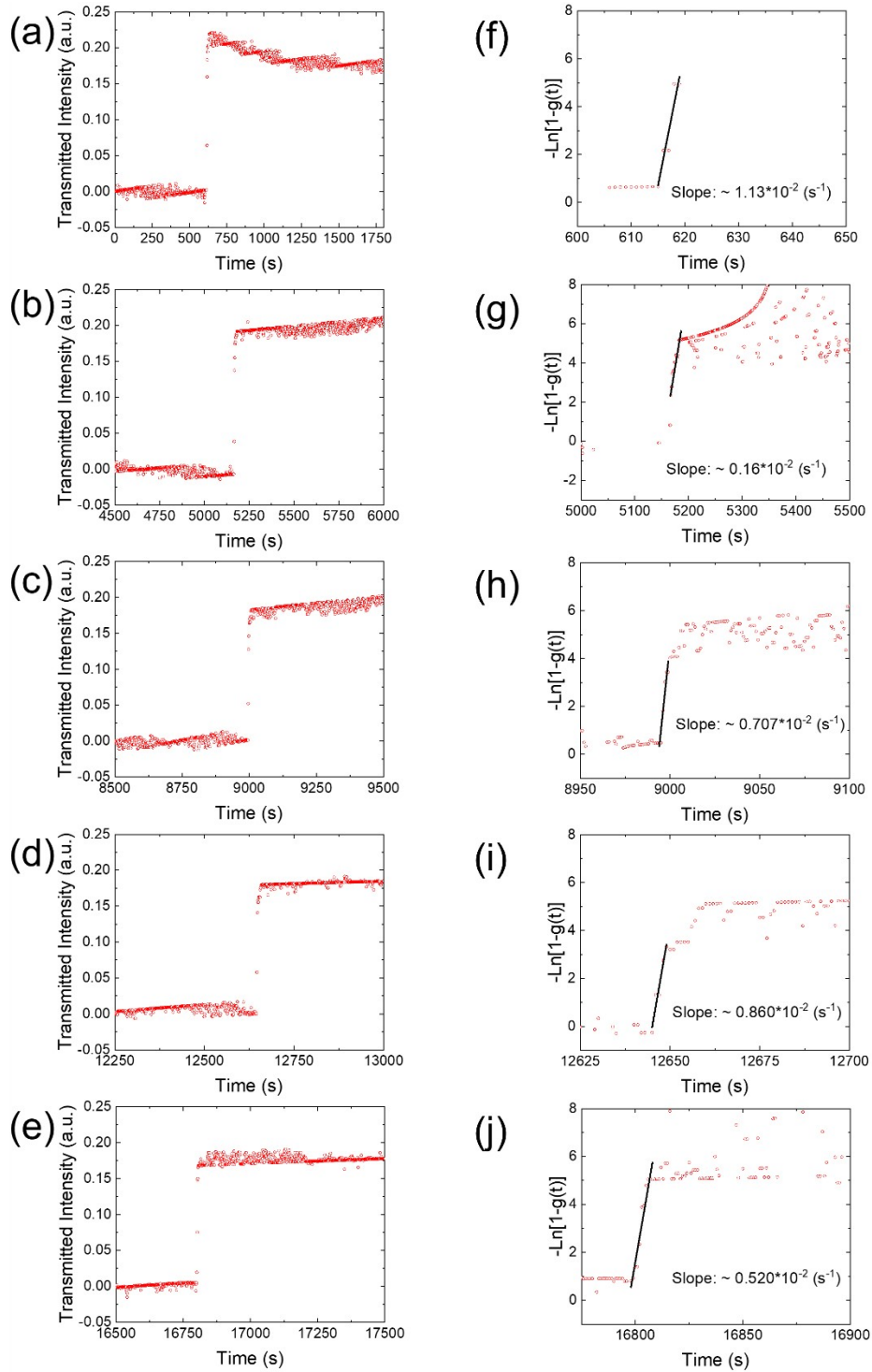
Supplementary Figure S11 Baseline-subtracted OTR curves (a)-(e) and corresponding fits (f)-(j) for the BPY thin film at a constant temperature of ~ 500 ˚C. In this case, since the relaxation times are comparable to the gas flush time for steam-switching, the apparent k values appear to be limited by the gas flush time rather than the intrinsic materials performance.
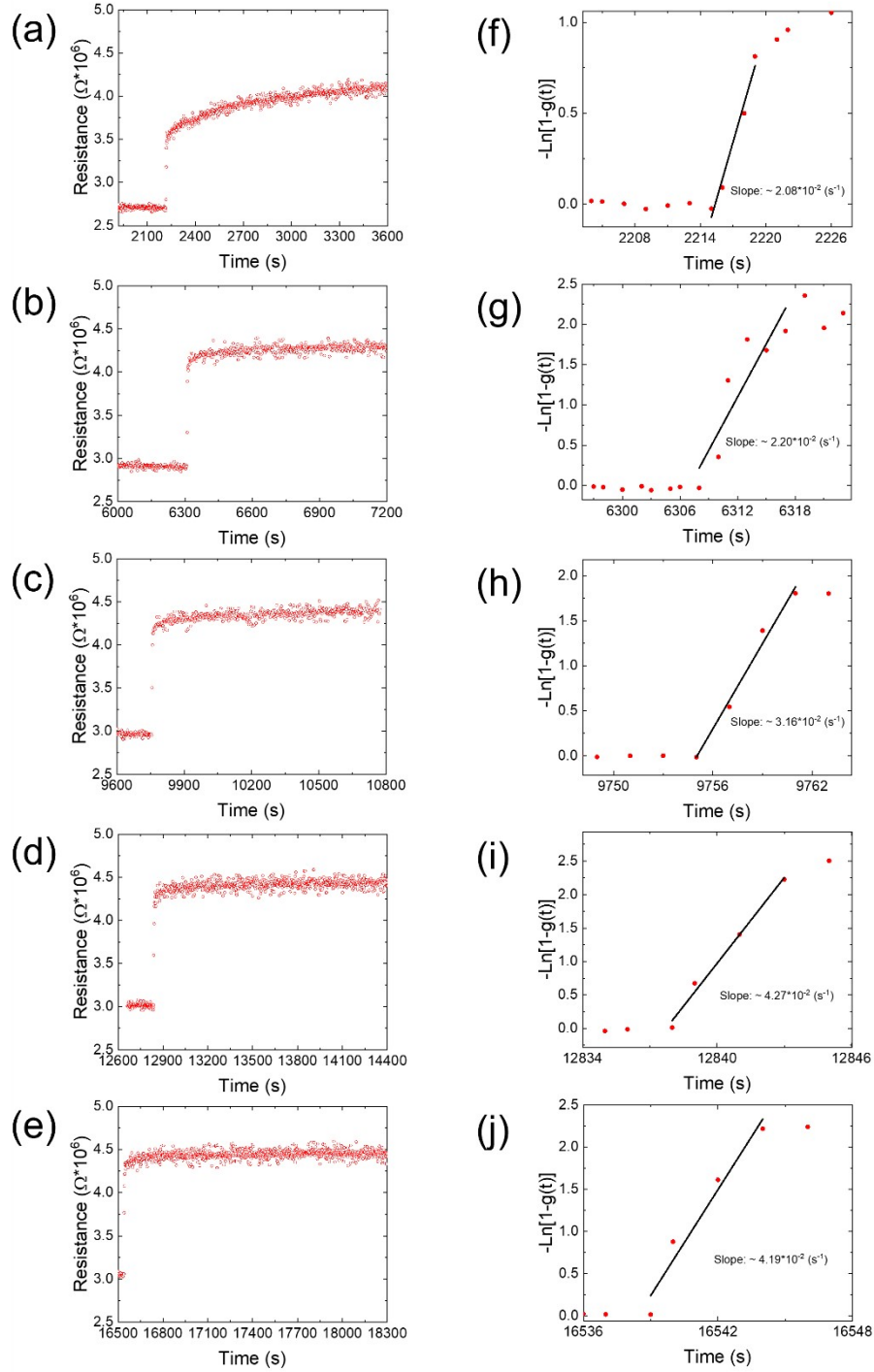
Supplementary Figure S12 Baseline-subtracted ECR curves (a)-(e) and corresponding fits (f)-(j) for the BPY thin film at a constant temperature of ~ 500 ˚C. In this case, since the relaxation times are comparable to the gas flush time for steam-switching, the apparent k values appear to be limited by the gas flush time rather than the intrinsic materials performance.

While the 2θ peak position shifted right about 0.1˚ after relaxation in the BCFZY thin film (out-of-plane contraction), there is very little 2θ peak shift after relaxation in BPY thin film as shown in **Supplementary Figure S13(a),(b)**. This result also suggests a possible structural/chemical change in the BCFZY film during the process of intermediate-temperature measurements; on the other hand, it could be caused by something as simple as a different H content or slightly different oxidation state compared to the as-grown composition.
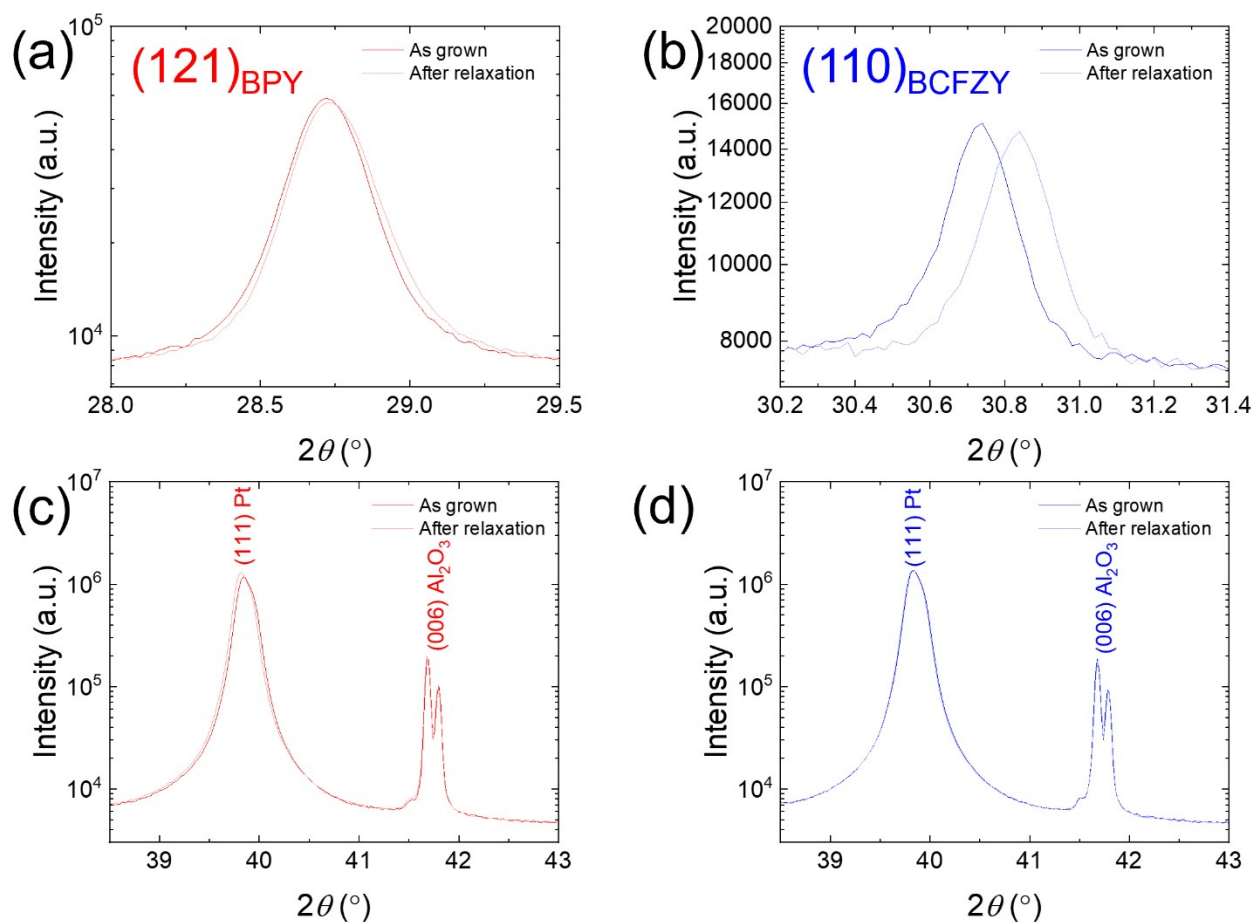
Supplementary Figure S13 (121) reflections of BPY thin film (a) and (110) reflections of BCFZY thin film (b) before and after steam relaxation, respectively. (c),(d) show XRD reflections around the Pt (111) (current collector) and Al_2O_3 (substrate) for the BPY and BCFZY thin films, respectively.
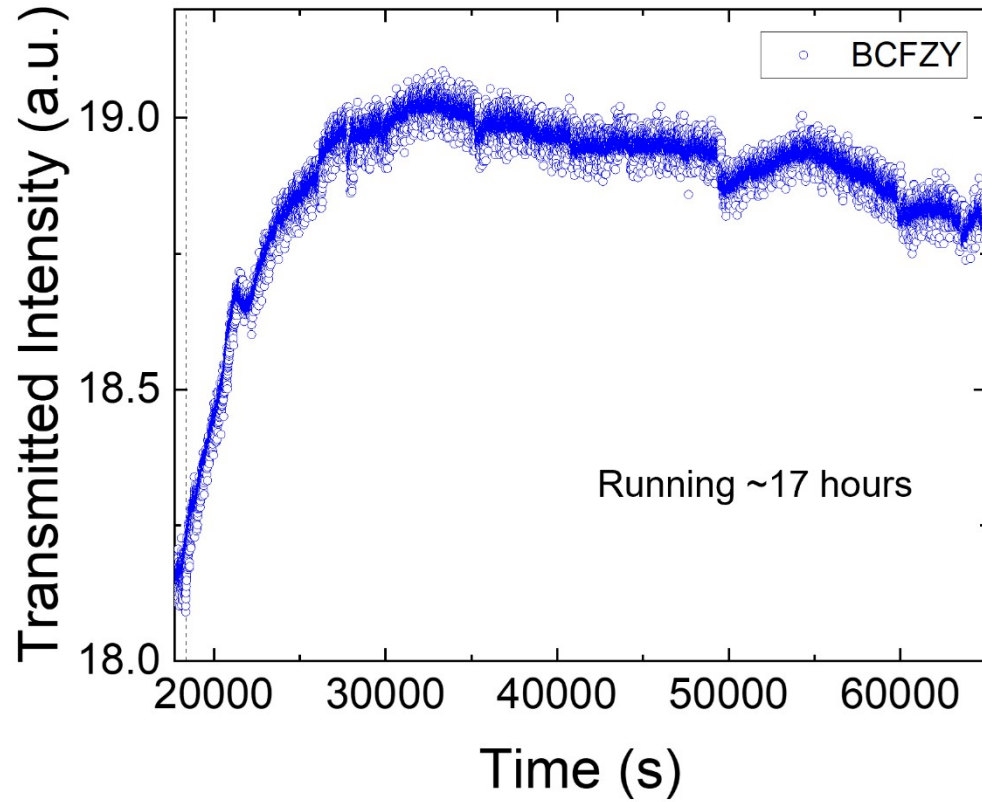
**Supplementary Figure S14** OTR curve of long-term steam (2.3 % H_2O)-exposed BCFZY film for sample preparation of STEM measurements at a constant temperature of approximately 400 ˚C. Dashed line indicates the steam switching (0 to 2.3% H_2O).
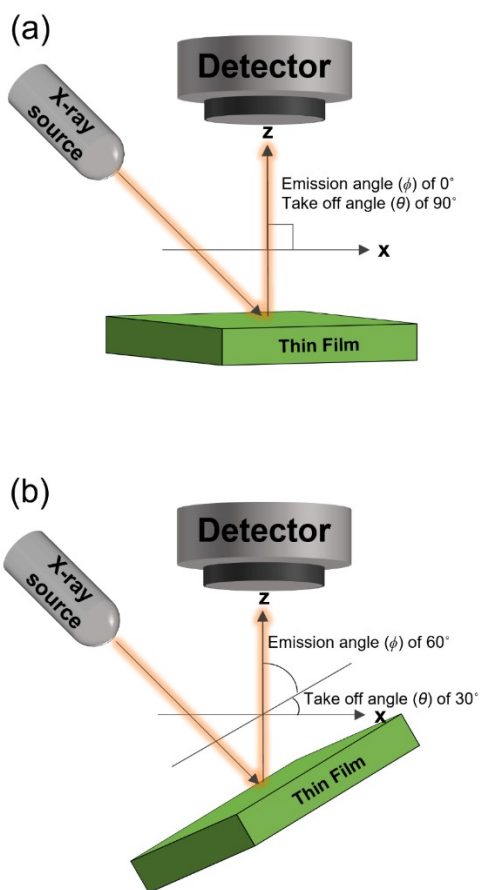
Supplementary Figure S15 Schematic of XPS measurements at two distinct X-ray take-off angles of 90 (a) and 30° (b), respectively.

Table S1 Inelastic electron mean free paths (IMFP) and analysis depth calculation at $\theta = 30°$ depending on elements of the BCFZY and BPY thin films. IMFP is calculated by using QUASES software from Tanuma, Powell, Penn formula. [7] Note that detection depth at $\theta = 30°$ is calculated by equation of $3*\text{IMFP}*\cos(\theta)$.

Compounds	3*IMFP at $\theta = 90°$	Detection depth at $\theta = 30°$
BaO_2	48 Å	7.41 Å
Co_3O_4	44.04 Å	6.78 Å
Fe_2O_3	49.56 Å	7.65 Å
ZrO_2	62.07 Å	9.57 Å
Y_2O_3	74.16 Å	11.43 Å
$PrCl_3$	40.11 Å	6.18 Å
SiO_2	109.38 Å	16.86 Å
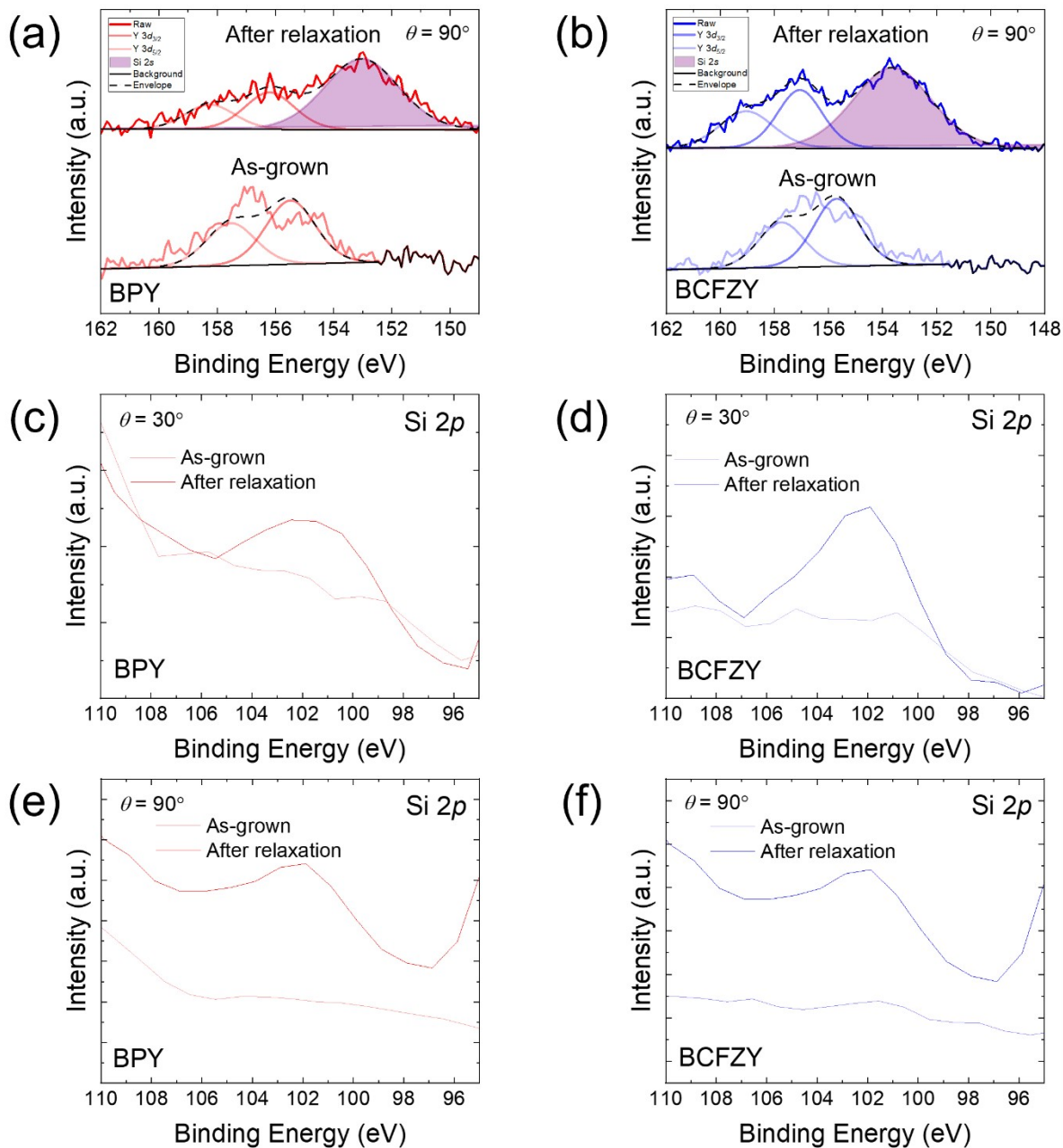
Supplementary Figure S16 XPS spectra of Y 3*d* and Si 2*s* for the BPY (a) and BCFZY (b) thin films. The data are recorded at take-off (*θ*) angle of 90˚. Si 2*p* XPS spectrum from full XPS spectrum recorded for take-off (*θ*) angles of 30 and 90˚ for the BPY (c),(e) and BCFZY (d),(f) thin films, respectively.
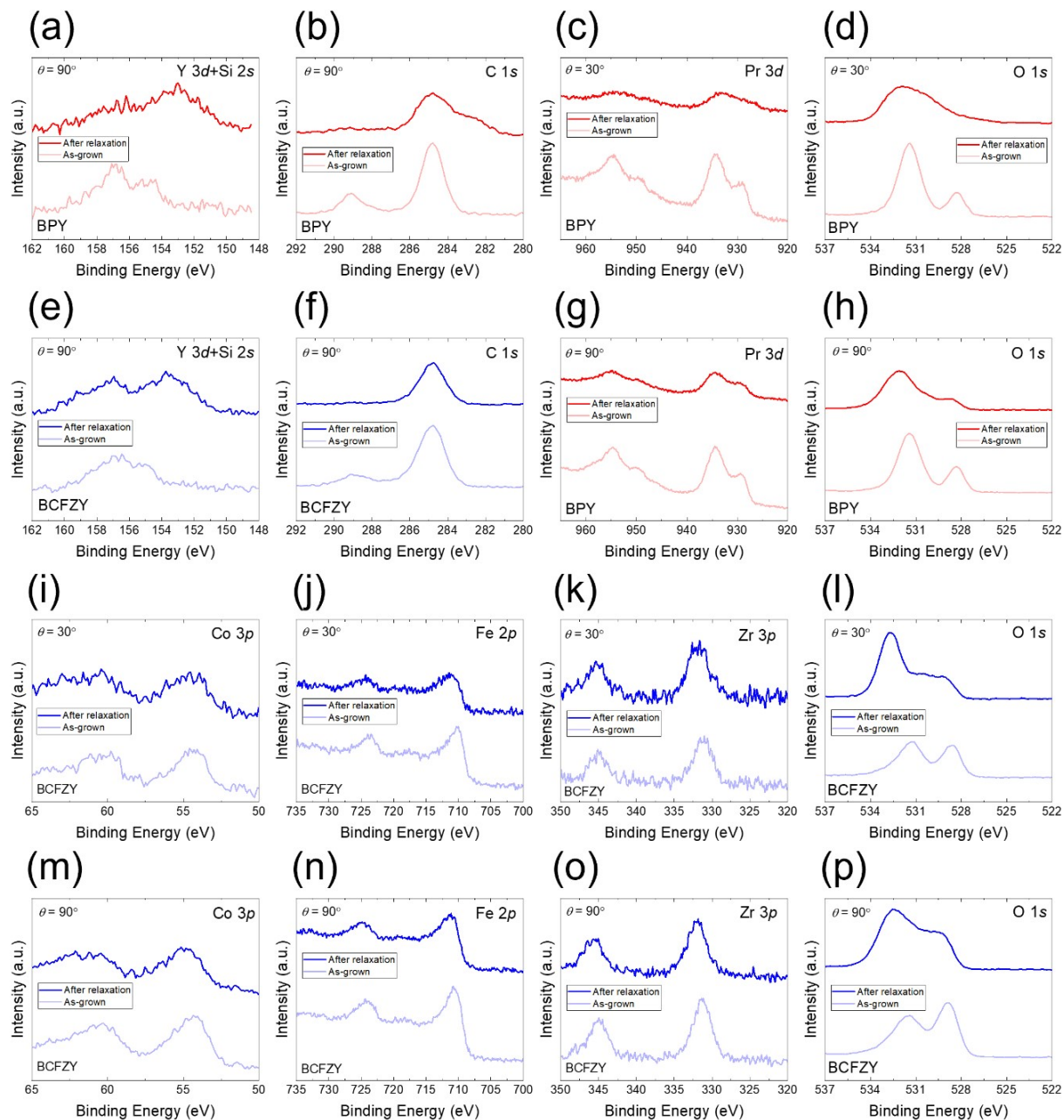
Supplementary Figure S17 XPS spectra of Y 3*d*, Si 2*s* regions and C 1*s* (b) recorded at take-off angle (*θ*) of 90˚ for the BPY (a),(b) and BCFZY (e),(f) thin films. XPS spectra of Pr 3*d* (c),(g) and O 1*s* (d),(h) recorded at take-off angle (*θ*) of 30 and 90˚, respectively, for the BPY thin film before and after steam relaxation measurements. Co 3*p* (i),(m), Fe 2*p* (j),(n), Zr 3*p* (k),(o), O 1*s* (l),(p) XPS spectra recorded at take-off angle (*θ*) of 30 and 90˚, respectively, for the BCFZY thin film before and after steam relaxation measurements.
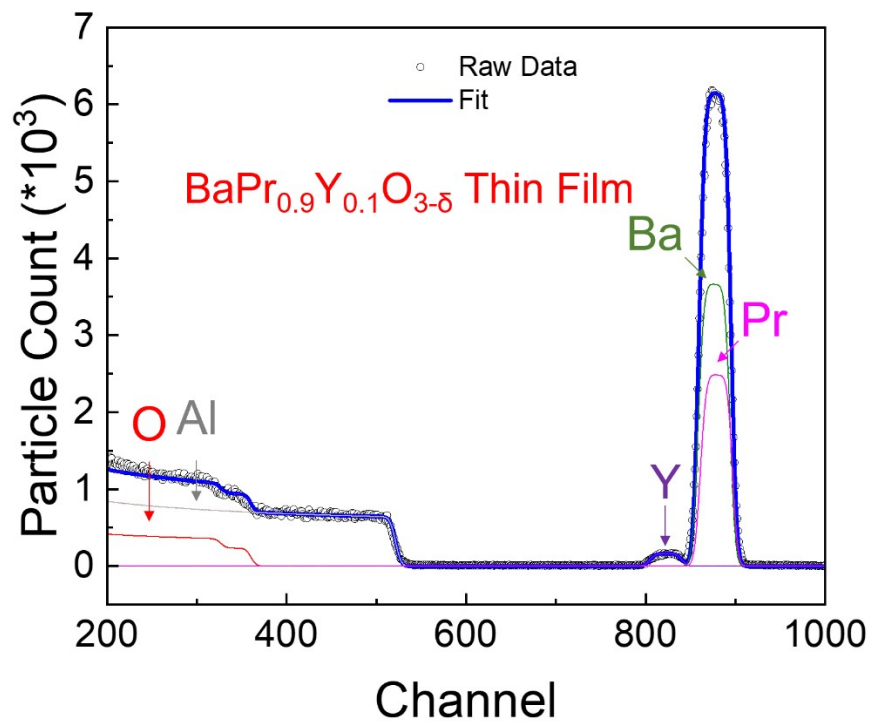
Supplementary Figure S18 Rutherford backscattering spectrometry data and fitted lines of BPY thin film grown on sapphire substrate.
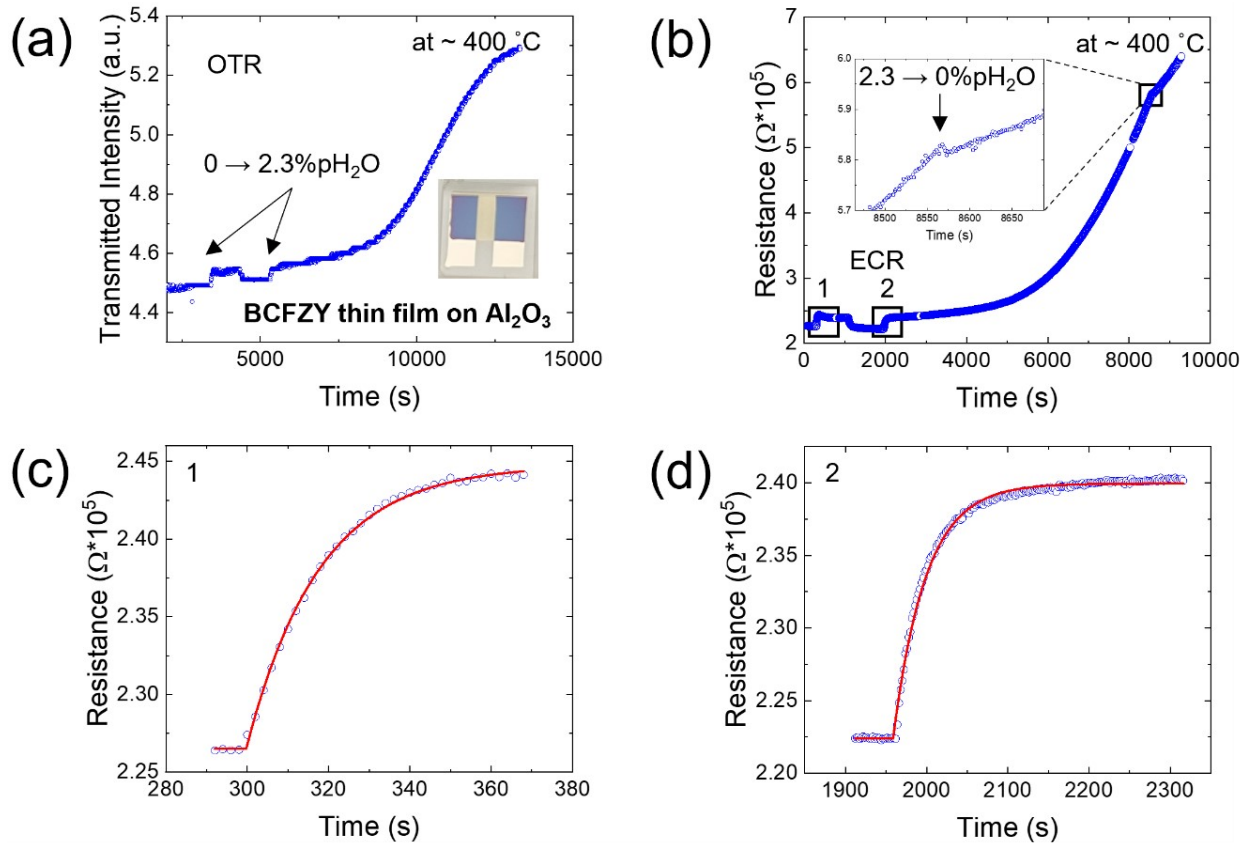
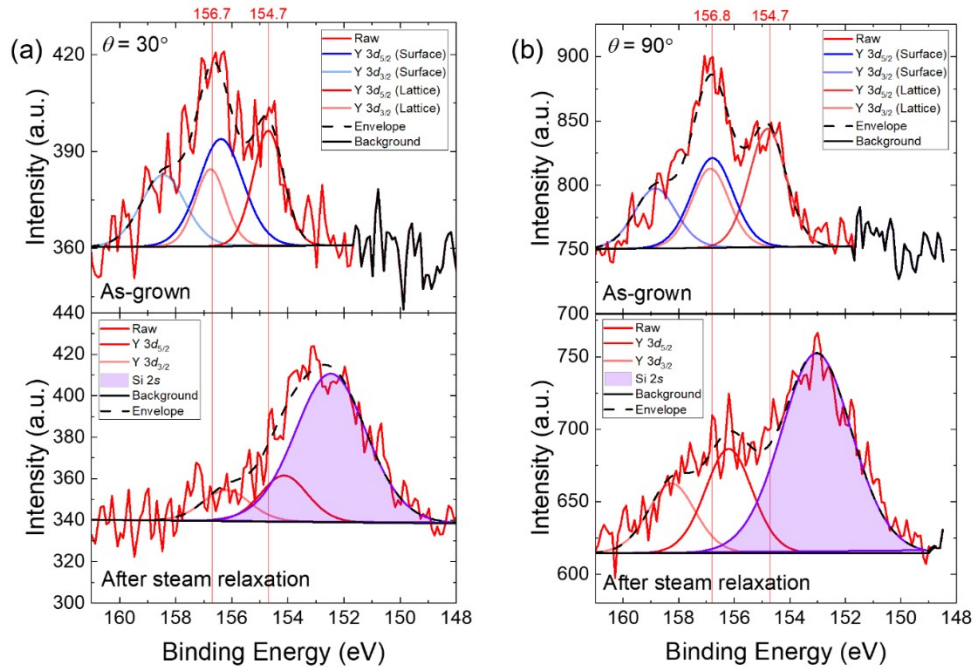**Supplementary Figure S19** OTR (a) and ECR (b) curves of BCFZY thin film grown at repetition rate of 20 Hz during steam switching as a function of time at a constant temperature of approximately 500 ˚C. Enlarged ECR curves of square 1 (c) and 2 (d) in Figure S21(b).

Table S2 Angle-resolved XPS Ba, Y 3d, and O 1s peak positions of as-grown BPY thin film at $\theta = 30$ and 90°. The spin orbit splitting doublets of Y $3d_{3/2}$ and $3d_{5/2}$ were fitted by a 2:3 peak area ratio with a binding energy separation of 2.05 eV. For the Ba 3d spectra, we kept energy separation of 15.33 eV with a 2:3 peak area ratio between $3d_{3/2}$ and $3d_{5/2}$. [8]

	Ba $3d_{3/2}$				Note
	As-grown		After Steam Relaxation		
$\theta = 30°$	Surface	Lattice	Surface	Lattice	
Peak Position	796.1 eV	795.6 eV	796.5 eV	795.0 eV	
Concentration	5.89%	33.86%	16.78%	22.97%	
$\theta = 90°$	Surface	Lattice	Surface	Lattice	
Peak Position	796.1 eV	795.6 eV	796.5 eV	-	
Concentration	4.00%	35.75%	17.95%	-	

	Ba $3d_{5/2}$				Note
	As-grown		After Steam Relaxation		
$\theta = 30°$	Surface	Lattice	Surface	Lattice	
Peak Position	780.8 eV	780.2 eV	779.7 eV	781.2 eV	
Concentration	8.93%	51.32%	34.81%	25.44%	
$\theta = 90°$	Surface	Lattice	Surface	Lattice	
Peak Position	780.8 eV	780.2 eV	781.1 eV	-	
Concentration	6.07%	54.18%	27.21%	-	

	Y $3d_{3/2}$			Note
	As-grown		After Steam Relaxation	
	Lattice Y	Surface Y		
$\theta = 30°$ Peak Position	156.7 eV	158.4 eV	156.2 eV	Y ratio is significantly decreased by Si contamination after steam relaxation
Concentration	16.92%	23.06%	1.92%	
$\theta = 90°$ Peak Position	156.8 eV	158.8 eV	158.2 eV	
Concentration	21.56%	18.41%	3.17%	
$\theta = 90°$ Peak Position	157.2 eV [9]		-	Y'$_{Zr}$ in as-grown BZY, reference [9]

	Y $3d_{5/2}$			Note
	As-grown		After Steam Relaxation	
	Lattice Y	Surface Y		
$\theta = 30°$ Peak Position	154.7 eV	156.4 eV	154.1 eV	Y ratio is significantly decrease by Si contamination after relaxation
Concentration	25.40%	34.62%	2.89%	
$\theta = 90°$ Peak Position	154.8 eV	156.8 eV	156.2 eV	
Concentration	32.38%	27.65%	4.76%	
$\theta = 90°$ Peak Position	155.1 eV [9]		-	Y'$_{Zr}$ in as-grown BZY, reference [9]

	O 1s							Note
	As-grown			After Steam Relaxation				
$\theta = 30°$	Lattice	Hydroxide	Water	BaO	Lattice	Hydroxide	Water	
Peak Position	528.3 eV	531.4 eV	533.5 eV	527.7 eV	529.9 eV	531.5 eV	532.7 eV	
Concentration	19.24%	78.06%	2.7%	8.58%	27.19%	39.47%	37.26%	
$\theta = 90°$	Lattice	Hydroxide	Water		Lattice	Hydroxide	Water	
Peak Position	528.3 eV	531.4 eV	533.6 eV	✕	529.0 eV	531.3 eV	532.5 eV	
Concentration	22.82%	75.00%	2.18%		17.79%	31.99%	50.21%	

**Table S3** Area and ratio of Ba $3d_{5/2}$ spectra between surface and lattice Ba

Ba $3d_{5/2}$	Area (Surface)	Area (Lattice)	Ratio (Surface/Lattice)
$\theta = 30°$ (as-grown)	1858.1	10673.7	0.174
$\theta = 90°$ (as-grown)	3069.6	27407.5	0.112
$\theta = 30°$ (after relaxation)	6191.8	4528.6	1.367
$\theta = 90°$ (after relaxation)	31084.7	0	ꝏ

Supplementary Figure S20 Y 3*d* spectra and fitted curves of BPY thin films measured at $\theta = 30$ (a) and 90˚ (b) before (below) and after (above) steam relaxation.
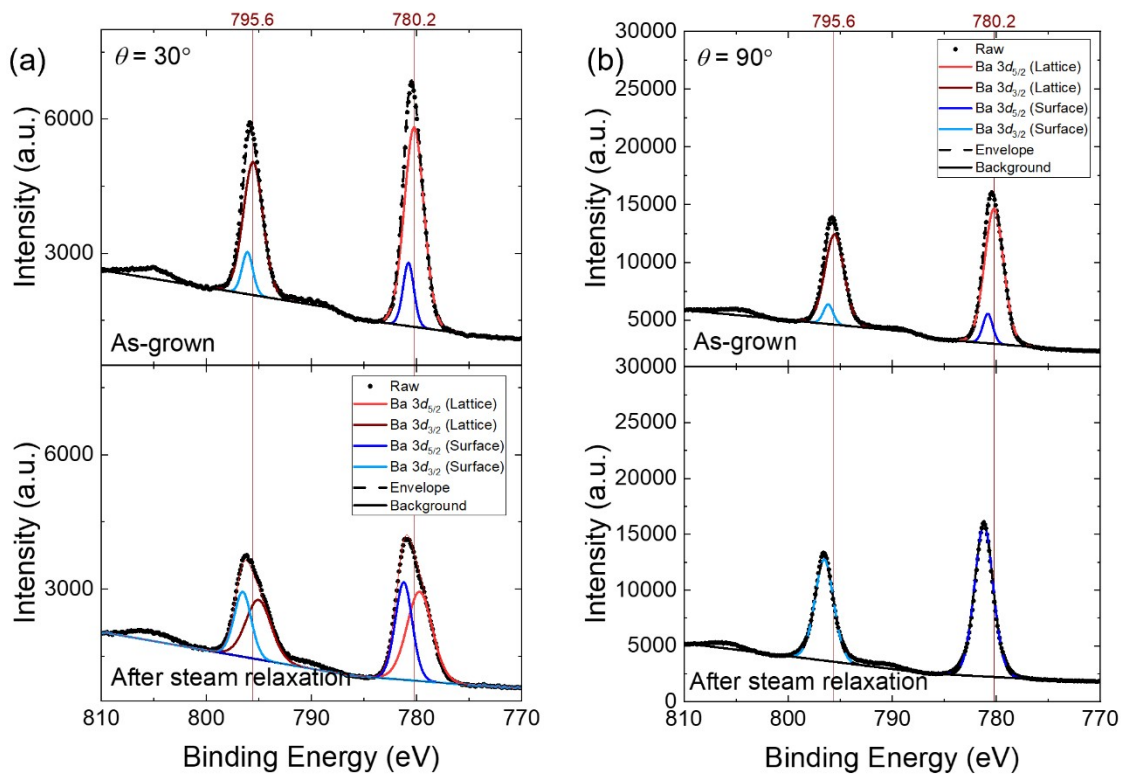
Supplementary Figure S21 XPS spectra and fit curves of Ba $3d$ at take-off (θ) angles of 30 (a) and 90° (b) for the BPY thin film before (top) and after (bottom) steam relaxation, respectively.
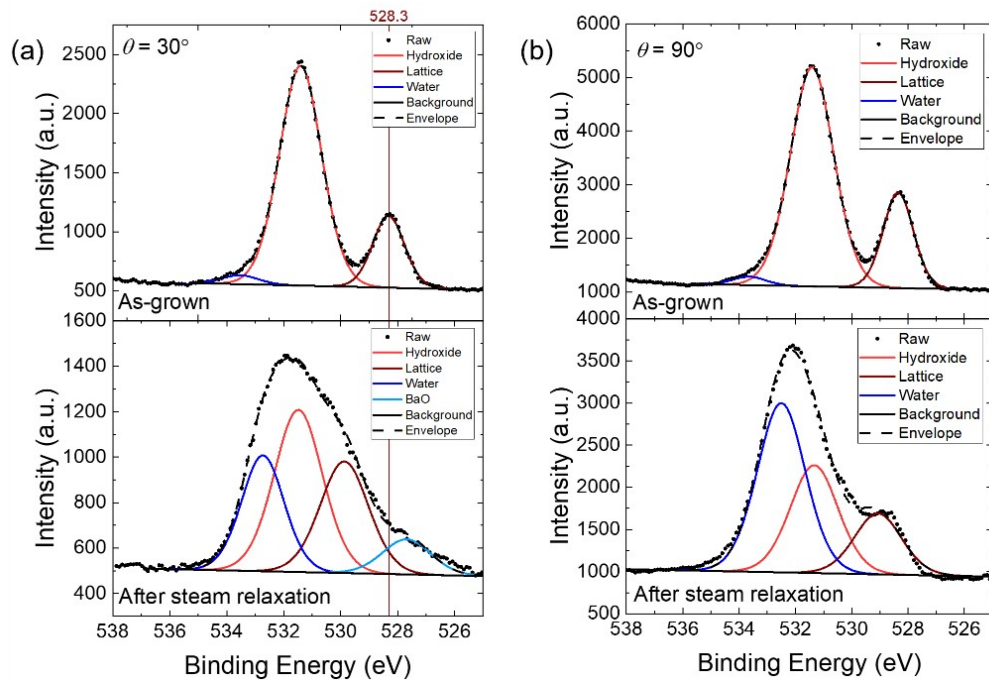
Supplementary Figure S22 XPS spectra and fit curves of O 1s at take-off (θ) angles of 30 (a) and 90˚ (b) for the BPY thin film before (top) and after (bottom) steam relaxation, respectively.

References for Supporting Information

[1] N. H. Perry *et al.*, Chem. Mater. 2019, **31**, 1030

[2] H. B. Buckner *et al*., Adv. Mater. Interfaces 2019, 1900496

[3] M. Schrade *et al.*, J. Am. Ceram. Soc. 2015, 99, 492

[4] L. O. Anderson *et al*., Chem. Mater. 2021, **33**, 8378

[5] A. X. B. Yong *et al*., J. Mater. Chem. A, 2023, **11**, 4045

[6] D.-K. Lim *et al*., Journal of Alloys and Compounds, 2014, **610**, 301–307

[7] S. Tanuma, C. J. Powell, D. R. Penn: Surf. Interf. Anal. 1994, **21**, 165

[8] J. Chastain and Roger C. King Jr. "Handbook of X-ray photoelectron spectroscopy." Perkin-Elmer Corporation, 1992, **40**, 221

[9] Y. Wang *et al*., J. Phys. Chem. C, 2023, **127**, 8937–8945